THE JOURNAL OF PHYSICAL CHEMISTRY B

Article

pubs.acs.org/JPCB

Hydration Effects on the Structural and Vibrational Properties of Yttrium Aluminosilicate Glasses for in Situ Radiotherapy

Jahangir Malik and Antonio Tilocca*

Department of Chemistry, University College London, 20 Gordon Street, London WC1H 0AJ, United Kingdom

ABSTRACT: The performances of silicate glasses as containment matrices or vectors of radioactive ions in nuclear waste storage and in situ radiotherapy are influenced by the effect of interstitial water on the glass durability. In order to assess how hydration determines changes to atomistic structural features which control the glass degradation, we have carried out molecular dynamics simulations of a typical yttrium aluminosilicate (YAS) glass employed in radiotherapy, incorporating different water contents. The analysis of the models allows us to discuss the way in which hydroxyl groups are distributed in the glass structure and modify or disrupt the aluminosilicate glass network. Hydration affects the silicate and aluminate connectivity to a different extent, resulting in a different degree of disruption (depolymerization) of the Si and Al network. The simulations also highlight a strong tendency of all hydrated compositions to form Y^{3+}- and OH^--rich domains, separated from the aluminosilicate matrix. The implications of these structural effects for the durability and ion release behavior of the glass are discussed, as well as the vibrational signatures of the various hydrous species identified in the models.

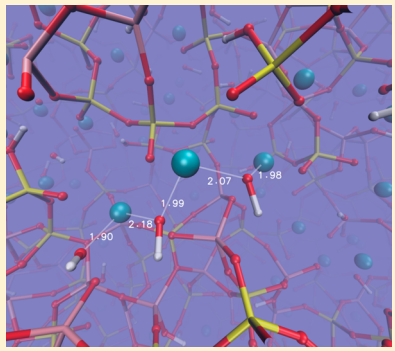

INTRODUCTION

Water affects the behavior of silicate glasses in many practical applications. For instance, biomedical applications rely on a fast dissolution of the glass in an aqueous biological medium, with release of soluble species such as calcium and silica ions which appear to regulate cellular activity, leading to tissue regeneration.[1,2] On the opposite side, water corrosion represents an unwanted process for the use of silicate glasses as optical fibres,[3] or as a matrix for hosting radionuclides, both for nuclear waste disposal and for in situ (internal) radiotherapy.[4−6] In the latter applications, the stability of the glass matrix over intermediate to long time scales is critical. In particular, internal radiotherapy applications involve a stable biocompatible vector (such as aluminosilicate glass microspheres[5]) to transport and deliver activated radioisotopes such as ^{90}Y directly into a tumor.[7] In this way, the target can be directly and safely hit by higher radiation doses, compared to external radiotherapy (whose highest allowed dose is limited by the need to prevent damage to surrounding healthy tissues), making in situ radiotherapy more effective for the treatment of deep-seated cancers.[8] The glass carrier must be stable in the aqueous biological environment long enough to prevent release of radioactive ions in the bloodstream during the treatment and before their decay (at least 2−3 weeks after injection): this vital requirement underpins the key role played by water−glass interactions for this application. Using classical and ab initio molecular dynamics (MD) simulations,[9] we have previously identified structural features of yttrium aluminosilicate (YAS) glasses that affect the glass dissolution[10,11] and started to develop models able to employ these structural descriptors to predict the dissolution behavior of the glass based on its chemical composition.[12] The local coordination environment of yttrium ions is one of these structural features, as it obviously affects the yttrium mobility in the glass matrix and its eventual dissolution.[11] The unwanted release of radioactive yttrium ions will also be accelerated if the surrounding aluminosilicate (AS) glass matrix rapidly degrades and dissolves in the host: this rate of degradation depends on medium-range structural features of the glass, such as the connectivity of the aluminosilicate network and the aggregation of network modifier ions (Y^{3+} in the case of YAS) in clusters.[9,13] In particular, a highly cross-linked glass network will offer higher resistance to the dissolution compared to a fragmented one;[9,14] moreover, the formation of segregated ionic clusters of small size breaks the continuity of migration channels necessary for fast ionic transport[15,16] and thus opposes a rapid dissolution. The previous simulations have illustrated a way in which these effects could be combined and exploited to maximize the durability of YAS and other potential bioactive radionuclide vectors.[12,17]

The above studies probed the bulk structure of dry glasses quenched from the melt. The incorporation of even small amounts of water is known to have a dramatic influence on the physicochemical, electrical, and optical properties of silicate glasses.[18−23] This influence presumably reflects structural changes induced by interstitial water:[24] several studies have thus attempted to elucidate the state of water incorporated in silica-based glasses.[20,25−37] An important finding is that low (<2−4 wt % H_2O) water contents will mainly be present as OH groups originated by water dissociation at strained network sites,[20] whereas undissociated molecular H_2O will also be present at higher water contents, especially in glasses hydrated

Received: July 23, 2013
Revised: October 25, 2013
Published: November 11, 2013

dx.doi.org/10.1021/jp4073203 | J. Phys. Chem. B 2013, 117, 14518−14528

at lower temperature.[19,25] Neutron diffraction experiments showed that the formation of Si−OH groups introduces significant changes in the medium-range order of sodium silicate glasses, involving depolymerization in the second coordination shell of Si atoms.[26] The situation is less clear regarding the distribution of OH species and the way in which they modify the structure of an aluminosilicate glass. The interpretation of vibrational and NMR spectroscopy data is rather inconclusive: they have been interpreted in favor of Si−OH, bridging Si−OH−Al, Al−OH, and also free (that is, not bonded to either Si or Al) OH species.[29−37] The exact nature of OH incorporation in the glass is quite important in the context of the glass durability, as Si−OH and Al−OH species are expected to involve bond breaking and network depolymerization, whereas free OH and bridging Si−OH−Al are not. On the basis of NMR experiments, it has been proposed that the glass network connectivity is not modified, as hydroxyl species mainly associate to modifier cations or form bridging Si−OH−Al, rather than Si−OH or Al−OH bonds.[32] On the other hand, other NMR experiments on aluminosilicate glasses have been interpreted as indicating the presence of both Si−OH and Al−OH, as well as free OH:[33−35] the bonded T−OH species formed by breaking T−O−T bridges are dominant in more polymerized compositions, whereas free OH species become increasingly relevant in depolymerized compositions containing network-modifier cations of high field strength.[33,36] Moreover, no preferential clustering of OH species in hydrous aluminosilicate glasses was detected by NMR,[19] at variance with earlier diffraction and Raman data which highlighted the separation between anhydrous and water-rich domains.[37]

The above studies mostly involved silicate and aluminosilicate glass compositions containing alkali and alkaline-earth cations, which are of particular interest in geology and technology. Because in internal radiotherapy YAS glasses are immersed in an aqueous biological environment, the durability of the YAS glass is also critically affected by the water-induced depolymerization of the glass network and the corresponding distribution of OH species in the glass matrix. It is thus important to investigate the hydration of YAS glasses, in order to assess whether and how structural features of the dry material which affect the glass durability are influenced by dissolved water. Here we target this goal by analyzing the structure of dry and hydrated YAS glasses modeled through MD simulations. The computational procedure adopted to model the hydrated glasses involves the structural relaxation (by MD high-temperature annealing) of a mixture containing the oxide glass and the hydroxyl components.[38] This approach is certainly suitable to model the hydrated glasses of interest here. In fact, most of the systems discussed above deal with water present in melts or melt-derived (natural or synthetic) glasses, and hydrous samples formed upon exposure to ambient air or by hydration of anhydrous melt-derived glasses and subsequent heat treatment at high temperatures (∼1000 °C):[18,19,21,22,24−26,32] these systems can also be considered representative of hydrated yttrium aluminosilicate glass. A computational approach involving quenching melts containing an appropriate amount of hydroxyl groups is thus appropriate to reproduce the experimental samples and conditions mentioned above. In particular, the MD quenching procedure is essentially a simulated-annealing way to identify the final stable configurations where the added hydrous species resulting from water incorporation are accommodated in favorable sites within the glass. In other words, the MD models obtained in this way will provide a realistic representation of the outcome of the actual process in which low-concentration water diffuses within the glass and reaches a favorable site where it dissociates to hydrous reaction products that separate until they are trapped in a local minimum.[24,28]

It is worth noting that some hydration-related structural features such as those that we identify in the present models may also be of interest for understanding the properties of glasses obtained through wet processing routes, which play an important role in the biomedical field, due to their attractive features (easier processing and manufacturing, higher activity)[39] in alternative to conventional melt-derived glasses. However, because the present procedure does not reproduce key stages of the sol−gel synthesis (hydrolysis/condensation, gelation, particle agglomeration, aging, drying, and stabilization), the models will necessarily lack some characteristic features of sol−gel materials, such as the disordered array of interconnected nanopores which leads to a high internal surface area and corresponding high activity,[39] and they cannot be considered fully representative of sol−gel materials. Different approaches and force fields would be needed to reproduce the latter processes and features and obtain realistic models of a sol−gel glass.[40,41]

We have modeled a highly representative YAS composition incorporating different hydration levels, and compared the hydrated structures to that of the corresponding dry glass. The results illustrate in detail how incorporation of water and hydration/hydroxylation modify existing structural features and introduce new effects which should be taken into account when exploring the use of YAS and related vectors for applications which rely on the durability of the glass.

SIMULATION METHODS

All glass structures were obtained through classical MD simulations with the DL_POLY code,[42] using a shell-model potential based on the SM1 force field originally derived to model modified phosphosilicate glasses.[43,44] Full (formal) ionic charges are employed for each ionic species except the O and H belonging to hydroxyl groups, for which we employ fractional charges of −1.4 and +0.4, previously derived from quantum chemical calculations of inorganic oxides.[45] All oxygen species are treated as core−shell units, with the total negative charge Z split between core (of charge +Y) and shell (of charge Z − Y); see Table 1. In addition to Coulomb interactions and core−shell harmonic forces acting on each oxygen, the original SM1 potential includes Buckingham terms to describe van der Waals interactions between all cations and oxygen shells O_S, and truncated three-body terms controlling O−Si−O angles. The present systems introduce additional interactions, for which new parameters were obtained. The Al−O_S Buckingham potential parameters were those of ref 46; new Buckingham terms for Y−O_S interaction were obtained by fitting to the crystal structures of yttrium silicate and aluminate structures, using the GULP code,[47] and were recently employed to model yttrium-doped bioactive glasses.[13] Hydroxyl species were represented by the Baram−Parker potential,[45] involving a core−shell harmonic potential on the oxygen and a Morse function describing the Oh_S−H bond (where Oh_S is the hydroxyl oxygen shell), plus additional Buckingham terms for the Oh_S interactions with Si, Al, and O_S.[45,46] These OH parameters had been fitted to ab initio results[45] and have been successfully employed in a very large number of simulations of hydrated aluminosilicate and aluminophosphate sys-

dx.doi.org/10.1021/jp4073203 | J. Phys. Chem. B 2013, 117, 14518−14528

Table 1. Interatomic Potential Terms and Parameters

Core–Shell Harmonic Potential: $V(r) = 0.5kr^2$			
interaction	k (eV Å^{-2})		
$O_C^{0.8482}$–$O_S^{-2.8482}$	74.92		
$Oh_C^{0.9}$–$Oh_S^{-2.3}$	74.92		
Buckingham Potential: $V(r) = Ae^{-r/\rho} - Cr^{-6}$			
interaction	A (eV)	ρ (Å)	C (eV Å^6)
O_S–O_S[43]	22764.3	0.149	27.88
Si–O_S[43]	1283.91	0.32052	10.66158
Si–Oh_S[46]	983.556	0.32052	10.66158
Al–O_s[46]	1460.3	0.29912	0
Al–Oh_S[46]	1142.6775	0.29912	0
Y–O_S[13]	1444.836	0.347	0.1
Y–Oh_S[this work]	886.85	0.347	0.1
Oh_S–O_S[45]	22764.3	0.149	13.94
Oh_S–Oh_S[45]	22764.3	0.149	6.97
O_S–H[46]	311.97	0.25	0
Oh_S–H	311.97	0.25	0
Morse Potential: $V(r) = D[1 - \exp(-\beta(r - r_0)]^2$			
interaction	D (eV)	β (Å^{-1})	r_0 (Å)
O_S–H[45]	7.0525	3.17490	0.9485
Three-Body Potentials $V^{OSiO}(\theta_{ijk}) = 0.5k(\theta_{ijk} - \theta_0)^2 \exp[-(r_{ij}^8 + r_{ik}^8)/\rho^8]$; $V^{OAlO}(\theta_{ijk}) = 0.5k(\theta_{ijk} - \theta_0)^2 \exp[-(r_{ij} + r_{ik})/\rho]$			
interaction	k (eV rad^{-2})	θ_0 (deg)	ρ (Å)
O—Si—O (O = O_S, Oh_S)	6.150	109.47	1.95
O—Al—O (O = O_S, Oh_S)	100.0	109.47	1.0

tems.[46,48−50] Finally, the Y–Oh_S interaction parameters were obtained by refitting the Y–O_S ones described above through the auxiliary charges approach[46] to take into account the different charges of O_S and Oh_S (see Table 1). Screened three-body terms controlled all O–T–O angles, where T = Si or Al and O = O_S or Oh_S.

The core–shell dynamics was controlled through adiabatic MD,[51] which requires assigning to the shells a small fraction (0.2 amu in this case) of the oxygen mass and integrating the equations of motion through a correspondingly small (2×10^{-4} ps) time step. The dry glass model was obtained following the same procedure as in previous MD simulations with the SM1 potential.[13] An initial array of ∼2000 atoms reflecting the YAS17 composition (17% Y_2O_3; 18.9% Al_2O_3; 64.1% SiO_2) was randomly arranged in a cubic box of size appropriate to yield the correct density of the glass,[13] and then heated up and held at 3500 K in a 200 ps trajectory at a constant number of particles, volume, and temperature (NVT ensemble). A Berendsen thermostat with a relaxation time of 0.2 ps was employed in all runs. The melt is then rapidly cooled down to room temperature at a cooling rate of 10 K/ps, and the glass so formed is further equilibrated in a final 200 ps NVT run at 300 K, from which structural properties are extracted.

Hydrated glasses of nominal compositions $(Y_2O_3)_{0.17}(Al_2O_3)_{0.19}(SiO_2)_{0.64}(H_2O)_z$ with z = 0.05, 0.1, and 0.15 were modeled, corresponding to low water contents, between 0.9 and 2.7 wt % H_2O. Only hydroxyl groups but no molecular water were included, reflecting the dominance of OH groups at low water content in melt-based aluminosilicate glasses,[19] and also in sol–gel bioglasses stabilized at moderate temperatures.[38,39] As the experiments clearly show that, for the low water contents considered here, all water is present as hydroxyl groups, our effective approach should lead to a realistic model in this case. For the compositions and water contents that we are investigating, a different approach in which molecular water is introduced and allowed to dissociate through a reactive potential[52] is expected to lead to a similar fully dissociated realistic sample, and therefore would not provide any specific advantage in this case. On the contrary, there is the possibility that, starting from a sample containing molecular water, dissociative (kinetic) barriers may hinder the formation of a fully dissociated sample (correctly reflecting the experimental data) within the intrinsically limited MD time scales: the present approach also overcomes this potential issue of all MD simulations. A reactive potential, if adequately combined with enhanced-sampling techniques to overcome the dissociative barriers, would certainly be more useful for other systems where the actual ratio of molecular vs dissociated water is less well-defined or not defined at all.

The density of the hydrated glasses was fixed to that of the dry YAS17 glass. Because no clear-cut data are available on the dependency of the density on the OH content for these materials, it is much preferable to use this approximation rather than modifying the density based on some uncertain assumption about the unknown specific density dependence. Moreover, to further validate this approach, we have checked that no significant changes to the reported structures and trends occur when the density of the hydrated system is changed by ±3%, as could be expected on the basis of the low OH content.

The corresponding atomic compositions $[Y_{0.34}Al_{0.38}Si_{0.64}O_{2.36-z}(OH)_{2z}]$ are labeled according to the OH content: for instance, $YAS_{0.1}$ represents the YAS17 composition where 0.1 OH^- groups have replaced z = 0.05 O^{2-} ions per formula unit. Hydroxylated structures were generated starting from a random initial configuration that included the required number of OH groups, with minimum distance constraints in place to prevent initial overlaps with other atoms. In order to avoid any bias on the final structure due to a specific initial arrangement of OH groups, an array of nonoverlapping OH groups was randomly distributed in the simulation box first, before arranging the remaining atoms within the remaining space. Moreover, to avoid problems related to the sensitivity of the core–shell dynamics of hydroxyl oxygens to the initial highly distorted configurations far from equilibrium, the OH positions were initially fixed, while allowing the other atoms to relax around them in a short initial minimization. Thereafter, the OH groups were released and the full system was slowly heated up to 900 K in three NVT runs at T = 300, 600, and 900 K, of 300 ps each. The length of each run was sufficient to equilibrate the system at the corresponding temperature, as checked by observing the convergence of the configurational energy in each case. Heating to 900 K allows the system to efficiently explore the configurational space, removing unstable interactions before cooling back to room temperature and carrying out the final NVT production run at 300 K. A snapshot of the $YAS_{0.1}$ glass is shown in Figure 1.

RESULTS

Local Structure and Coordination. The X–O (X = Si, Al, Y) radial distribution functions (rdf's) in Figure 2 show that hydration does not lead to deep geometrical rearrangements in the first (oxygen) coordination shell of the cations. The overall X–O interaction (bottom panel) is separated into the contributions from hydroxyl (O^H, middle panel) and non-hydroxyl (O^{NH}, top panel) oxygen atoms. The bottom panel

dx.doi.org/10.1021/jp4073203 | J. Phys. Chem. B 2013, 117, 14518−14528

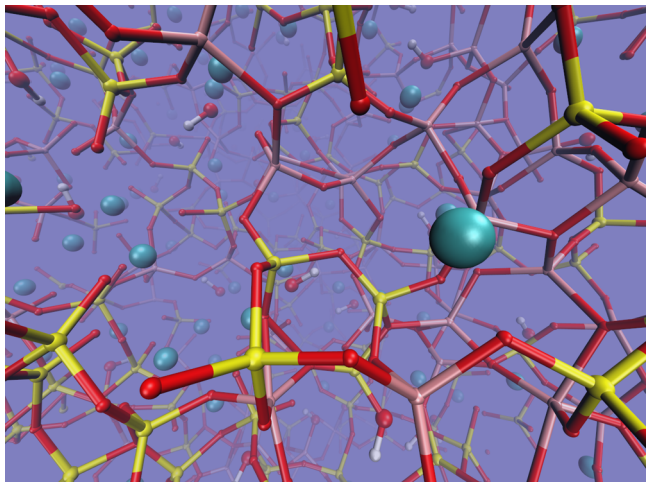

Figure 1. Snapshot of the $YAS_{0.1}$ glass. Si, Al, O, Y, and H are colored yellow, orange, red, cyan, and white, respectively.

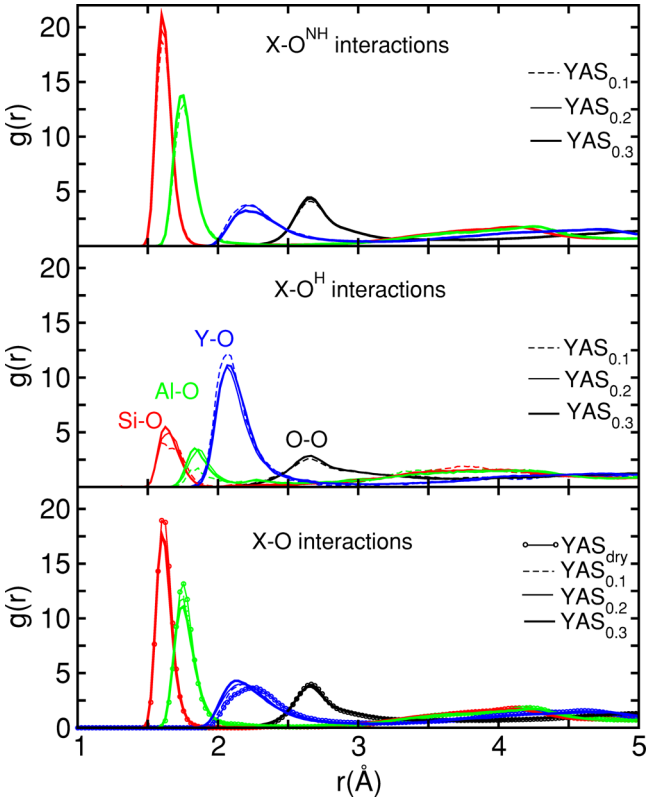

Figure 2. Radial distribution functions for X−O interactions (X = Si, Al, Y). The rdf's in the bottom panel include all interactions of X with any oxygen atom in the glass, whereas hydroxyl and non-hydroxyl components are shown in the middle and top panels, respectively.

shows that, compared with the structure of the dry glass, the main effect of the hydration is a slight decrease in the height of Si−O and Al−O peaks, accompanied by a slightly sharper Y−O peak, which is also shifted to shorter distances with respect to the dry glass (this shift is explained below). The middle and top panels highlight the dominant role of the X−OH interactions in inducing these changes to the coordination shell of Si, Al, and Y,[53] and also reveal a major OH contribution in the case of yttrium (see also Table 3).

Table 2 compares the X−O (X = Si, Al, Y) distances in the dry and hydrated glass, extracted from the rdf maxima of Figure 2. The distances in the dry glass are close to those obtained in previous simulations[10,11] and measured in experiments for related compositions.[54,55] In particular, the Y−O distance of 2.26 Å is in excellent agreement with the accurate prediction of YAS17 models obtained through ab initio molecular dynamics,[11] as well as with neutron diffraction measurements for yttrium aluminophosphate glass.[54] Hydrating the glass has no effect on the Si−O and Al−O distances. On the other hand, the Y−O distance gradually decreases to 2.13 Å, as a result of the contribution from shorter Y−O(H) distances, whose weight increases with OH concentration, as the OH fraction in the Y coordination shell increases (Table 3). Even though a split is also observed in the distances involving non-hydroxyl and hydroxyl oxygens for Si and Al, in this case, the average T−O distance is unaffected because the OH fraction in the Si/Al coordination shell is much lower compared to yttrium (Table 3).

Table 2. Si−O, Al−O, and Y−O Distances (i.e., Distance of the First Corresponding rdf Maximum in Figure 2)[a]

	interatomic distance (Å)		
	Si−O	Al−O	Y−O
composition	($Si-O^{NH}$, $Si-O^{H}$)	($Al-O^{NH}$, $Al-O^{H}$)	($Y-O^{NH}$, $Y-O^{H}$)
YAS17	**1.61**	**1.76**	**2.26**
$YAS17_{0.1}$	**1.60** (1.60, 1.64)	**1.76** (1.75, 1.85)	**2.19** (2.22, 2.07)
$YAS17_{0.2}$	**1.60** (1.60, 1.64)	**1.76** (1.75, 1.85)	**2.17** (2.22, 2.07)
$YAS17_{0.3}$	**1.60** (1.60, 1.62)	**1.76** (1.75, 1.85)	**2.13** (2.22, 2.07)

[a]The two numbers between parentheses are the distances to the corresponding non-hydroxyl and hydroxyl oxygen atoms, respectively.

Table 3. Percentage of X−OH (X = Si, Al, Y) Bonds in the X Coordination Shell

composition	%Si−OH	%Al−OH	%Y−OH
$YAS17_{0.1}$	2.9	2.4	11.3
$YAS17_{0.2}$	6.4	8.0	24.0
$YAS17_{0.3}$	8.8	10.3	32.1

The X−O coordination numbers (n_{X-O}, obtained as integrals of the corresponding rdf up to the first minimum) are plotted in Figure 3. The Si−O, Al−O, and Y−O coordination numbers in the dry glass are 4, 4.27, and 6.2, respectively. The shell-model force field employed here thus leads to an improved Al−O coordination number compared to our previous YAS17 models obtained using a rigid-ion potential:[10] in fact, while the latter produced a n_{Al-O} close to 4, n_{Al-O} values between 4.19 and 4.26 have recently been reported for YAS compositions close to YAS17, based on ^{27}Al NMR.[56,57] The present improvement seems to arise from a higher fraction (25 vs 5% in the previous simulations[10]) of 5- and 6-coordinated Al in the present model, which is again much closer to the experimental estimate (~20%).[57] It is interesting that the shell-model estimate falls halfway between the rigid-ion n_{Al-O} (4.05) and an ab initio (4.55) estimate obtained through Car−Parrinello MD simulations, which is probably affected by larger error bars due to the small size of the model.[11]

Figure 3 highlights that while OH groups enter the coordination shell of both Si and Al to a similar extent (see the $Si-O^{H}$ and $Al-O^{H}$ components) the total Si−O (O = O^{NH}

dx.doi.org/10.1021/jp4073203 | J. Phys. Chem. B 2013, 117, 14518−14528

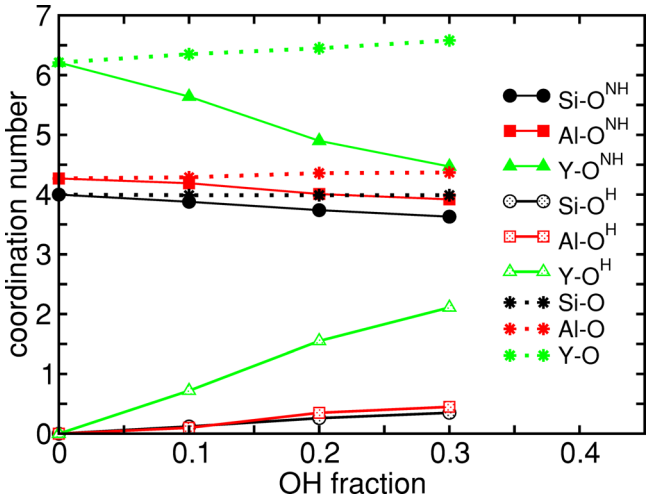

Figure 3. X–O coordination (X = Si, Al, Y). The dotted curves show the total ($X–O^{NH}$ plus $X–O^{H}$) coordination, whereas the $X–O^{NH}$ and $X–O^{H}$ components are shown as solid and empty symbols.

+ O^{H}) coordination always remains very close to 4, whereas that of Al slightly increases from 4.27 to 4.37. This reflects a more rigid SiO_4 tetrahedral environment, such that OH can bond to Si only by replacing one of the four oxygens (indicated by a corresponding decrease in the $Si–O^{NH}$ coordination in Figure 3). On the other hand, 5- or 6-coordinated species are more stable in the case of Al, and therefore, the formation of OH bonds can occasionally involve the expansion of a 4-fold Al coordination shell, hence the slight increase in total Al–O coordination. The strong Y–OH association noted before is now also quantitatively evident from Figure 3, showing that the average number of OH groups in the Y coordination shell ($n_{Y–OH}$) gradually increases to more than 2 for $YAS17_{0.3}$: this is accompanied by a marked decrease in the number of non-hydroxyl groups associated to Y, and an overall $n_{Y–O}$ going from 6.2 in the dry glass to 6.6 in $YAS17_{0.3}$.

Medium-Range Structure. Figure 4 describes the effect of hydration on the mutual distances between Si, Al, and Y atoms. The changes in the height of the rdf peaks denote a loss of Si–Al connectivity upon hydration, while Si–Si and Y–Y interactions are enhanced. The network connectivity (NC) of a network-forming species such as Si or Al is defined as the average number of bridging oxygen atoms (BOs) bonded to it.[58] One can also define "self" connectivities, which only involve bridges between two like species, i.e., Si–O–Si and Al–O–Al, and "cross" connectivities, which only involve bridges between two unlike species, i.e., Si–O–Al.[10,59] The partial connectivities count *all* A–O–B bridges from a central atom A to another atom B, even if some of these links share the same bridging oxygen O, as it occurs in the case of three-coordinated oxygen atoms. This definition then necessarily results in the sum of the partial connectivities higher than the A–O coordination number, and exceeding the total NC defined as the number of bridging oxygens bonded to A.[10] The Si–Si and Si–Al connectivities shown in Figure 5 reflect the trends suggested by the corresponding rdf peak heights in Figure 4. However, rather than the peak height, the X–Y connectivity must strictly reflect the area under the X–Y peak in the corresponding rdf. Whereas for the other pairs the peak height follows the same trend as the area under the peak, and is thus also representative of the connectivity, this is not the case for

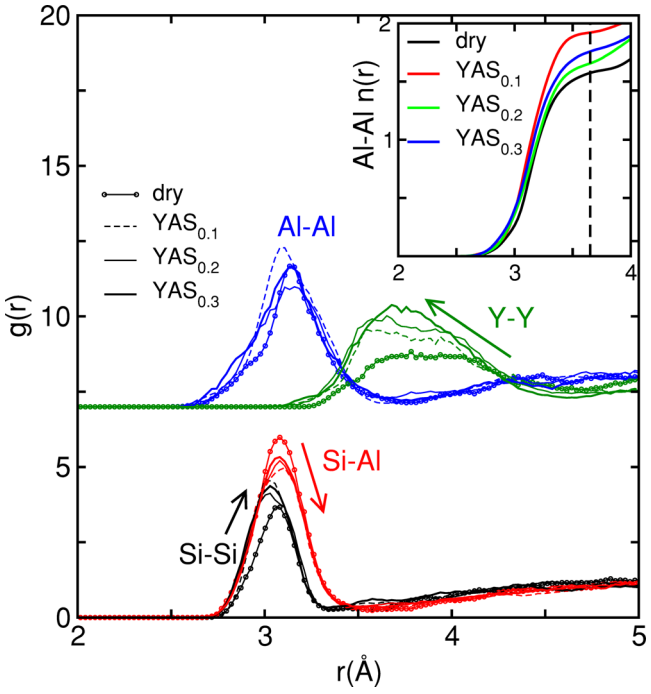

Figure 4. X–X (X = Si, Al, Y) radial distribution functions. The Al–Al and Y–Y rdf's are shifted vertically for clarity; the arrows highlight the observed trend with increasing hydration. The inset shows the running Al–Al coordination number (integral of the corresponding rdf's), with the dashed line denoting the radius of the Al–Al coordination sphere.

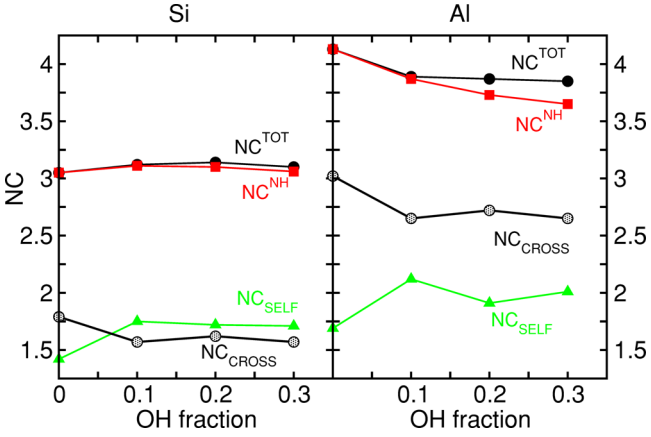

Figure 5. Total network connectivity of Si and Al (full circles) and self, cross, and non-hydroxyl components (triangles, open circles, and square symbols, see text for their definition).

the Al–Al peak height, due to the less regular peak shape. Instead, the trend of the Al–Al connectivity (NC_{self} in Figure 5) is closely reproduced by the running coordination number, shown in the inset of Figure 4, which shows that—as for the Si–Si case—hydration leads to a higher Al–Al connectivity with respect to the dry glass, even though no increase with OH amount is recorded: the highest NC_{self}(Al) is observed for $YAS_{0.1}$.

Figure 5 shows total NCs of 3.05 and 4.13 for Si and Al in the dry glass, respectively. The aluminum connectivity is higher than the corresponding value predicted by a rigid-ion potential,[10] reflecting the more realistic higher fraction of 5-coordinated Al in the present model, discussed above. Hydration has a different effect on the total Si and Al

dx.doi.org/10.1021/jp4073203 | J. Phys. Chem. B 2013, 117, 14518–14528

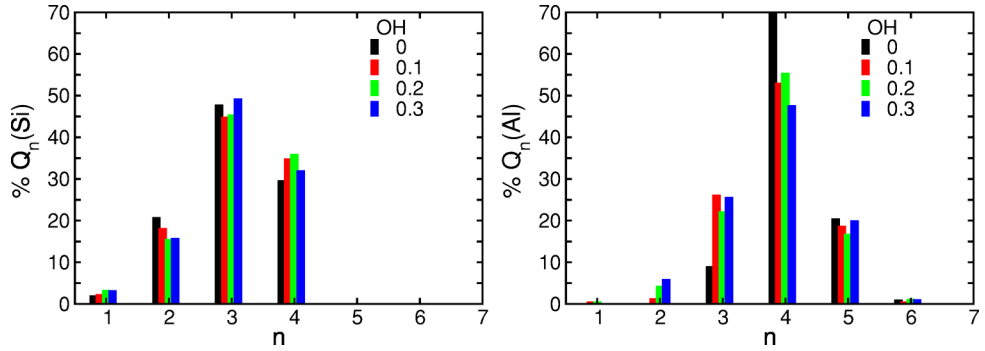

Figure 6. Q_n distribution for Si (left) and Al (right). The distribution for the dry glass is colored black.

connectivities: the first remains almost unchanged (increasing by 0.05 only), whereas NC(Al) decreases to ∼3.8. This can be understood through the self- and cross-connectivities in the same figure. These show that the Al connectivity in the dry glass is dominated by cross-links with Si, unlike the Si connectivity which is equally split between Si−Si and Si−Al links. As Figure 4 also suggested, formation of Si−OH and Al−OH bonds upon hydration mainly affects cross-links between Si and Al, whose amount decreases in favor of "self" Si−Si and Al−Al links. Due to their dominant weight in the case of Al, the loss of Si−Al cross-links upon hydration represents the main cause for the reduced Al network connectivity in the hydrated glasses, whereas for the same reason NC(Si) is largely unaffected. In particular, because the proportion of cross- vs self-links is much higher in the case of Al, a loss of these links will have a much bigger impact on the overall NC of Al, even in the presence of a higher number of Al−Al links: the latter are simply not enough to balance the dominant cross-connectivity, whose loss will then translate into a lower overall NC(Al). As a practical example, in the dry glass, each Al forms 3 links with Si atoms and 1.7 with another Al on average (see Figure 5), whereas each Si forms only 1.75 links to Al and 1.4 with another Si. The hypothetical rupture of all cross-links will leave a residual connectivity of 1.7 for Al and 1.4 for Si, that is a relative decrease in connectivity much more marked for Al, in spite of the higher Al−Al connectivity.

Another interesting feature emerging from Figure 5 is the presence of a small fraction of bridging hydroxyl (T−OH−T, T = Si, Al) groups.[32] T−OH−T bridges are revealed by any difference between the overall network connectivity calculated on all oxygen atoms (NC^{TOT}) and on non-hydroxyl O only (NC^{NH}): while almost no such hydroxyl bridges involve two Si, the figure suggests that a small but not negligible number of T−OH−T must involve Al: the presence of Al−OH−Al and Al−OH−Si structural units was confirmed by direct inspection of the models.

Figure 6 allows us to discuss in detail how the changes to the network connectivity discussed above reflect rearrangements in the underlying Q_n structure of Si and Al (Q_n species is a Si or Al atom bonded to n bridging oxygens). The very small increase in NC(Si) in the hydrated glasses reflects a lower Q_2 and a slightly larger Q_4 fraction. The marked overall decrease in the NC(Al) arises from $Q_4 \rightarrow Q_3$ and $Q_3 \rightarrow Q_2$ transformations: based on the previous discussion, these reflect formation of Al−OH bonds, mainly replacing broken Al−O−Si bridges.

Ion Clustering and Distribution of OH Groups. The extent of aggregation between two ionic species A and B in the glass can be assessed through the "clustering ratio" R_{AB} between the A−B coordination number n_{A-B} extracted from the simulations and the corresponding number that would be expected if ions B were uniformly (randomly) distributed around A, $4/3\pi R^3\rho_B$,[60] where R is the A−B cutoff distance (the first minimum in the corresponding rdf) and ρ_B is the number density of B atoms in the glass.[59] R_{AB} values higher than unity denote that a higher-than-random density of B ions populates the coordination shell of A, on average. The higher R_{AB}, the stronger the A−B association with respect to a random (i.e., no preference) situation. The clustering ratios in Figure 7(a)

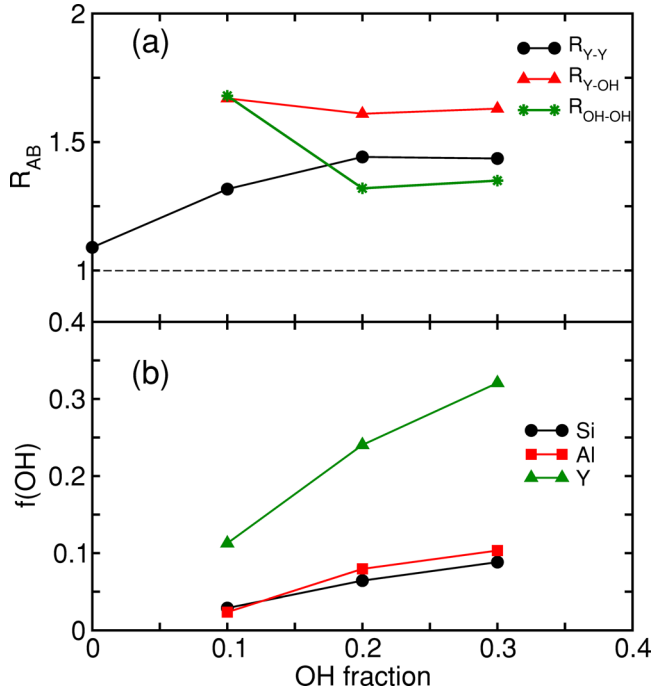

Figure 7. (a) Y and OH clustering ratios; (b) OH fraction in the oxygen coordination shell of Si, Al, and Y.

illustrate how Y and OH atoms are arranged in the glass matrix. Hydration leads to a marked increase in Y−Y clustering with respect to the OH-free YAS17; the R_{Y-OH} values in all hydrated compositions are also significantly higher than 1, suggesting that Y and OH always tend to aggregate with each other.

Further information on the hydroxyl distribution in the glass is provided in Figure 7b, plotting the hydroxyl component of the oxygen coordination shell of Si, Al, and Y. While these fractions obviously increase with OH concentration, the

dx.doi.org/10.1021/jp4073203 | J. Phys. Chem. B 2013, 117, 14518−14528

fraction of OH in the Si and Al coordination shells always remains rather low (going from 2% in composition $YAS_{0.1}$ to 10% in $YAS_{0.3}$) compared to the OH fraction around yttrium (11 to 32%).

The preferential Y−OH association emerged so far may favor the formation of segregated regions populated with "free" (i.e., not bonded to either Si or Al) OH and charge-balanced by Y^{3+} only. This possibility was tested by directly evaluating the total percentage of OH groups bonded to Si, to Al, or to neither Si nor Al, reported in Table 4: more than one-third of all OH

Table 4. OH Statistics: Percentage of OH Bonded to Si, Al, and Free (p_{OH-Si}, p_{OH-Al}, p_{OH-f}); p_{OH-Si}/p_{OH-Al} Ratio (to be Compared with N_{Si}/N_{Al} = 1.69); OH−Y Coordination Number (n_{OH-Y})

glass	p_{OH-Si}	p_{OH-Al}	p_{OH-f}	p_{OH-Si}/p_{OH-Al}	n_{OH-Y}
$YAS_{0.1}$	38.5	18.8	42.7	2.05	1.37
$YAS_{0.2}$	37.7	25.5	36.8	1.48	1.3
$YAS_{0.3}$	38.0	23.7	38.3	1.60	1.3

groups is in fact always found not bonded to either Si or Al. Because each OH is always coordinated to at least one Y^{3+} ion ($n_{OH-Y} > 1$ for all compositions), this entails that yttrium ions are still charge-balancing the "free" OH groups; that is, no truly isolated hydroxyls are present in the glass.

Table 4 also shows that, when a higher OH amount is incorporated in the glass, the fraction of Al-bonded OH increases, with a corresponding decrease in the fraction of free OH. The fact that additional Al−OH bonds are only formed at higher OH concentrations would seem to denote that Al−OH are always less favored than Si−OH bonds, whose fraction remains constant. However, one also has to take into account the nominal Si:Al ratio in the glasses, fixed to 1.69 in the three hydrated glasses, which means that there always is a higher number of Si than Al atoms available to bond OH. At the lowest OH concentration ($YAS_{0.1}$), the ratio of Si-bonded to Al-bonded OH is still higher than the nominal Si:Al ratio, whereas it becomes lower for $YAS_{0.2}$ and $YAS_{0.3}$. This means that hydroxyl groups are not randomly split among Si and Al: their partitioning is biased toward Si at the lowest water concentration and toward Al at higher OH concentration.

Vibrational Properties. The partial vibrational density of states (VDOS) of different atomic species was calculated as the Fourier transform of the corresponding velocity time autocorrelation function (VACF):[61]

$$\mathrm{VACF}_l(t) = \frac{1}{N_0 N_l} \sum_{j=1}^{N_0} \sum_{i=1}^{N_l} \vec{\mathbf{v}}_i(t_j)\cdot\vec{\mathbf{v}}_i(t_j + t) \quad (1)$$

where $\mathbf{v}_i$ is the velocity vector of the ith atom of species l, N_0 is the overall number of time origins spaced by time t in the MD trajectory, and $\mathbf{N}_l$ is the total number of atoms of species l. The bottom panel of Figure 8 shows the partial VDOS of each species in the hydrated $YAS_{0.3}$ glass. The characteristic vibrational frequencies of each species can be linked to IR and Raman spectroscopy assignments. The low-frequency region of the spectrum (below 300 cm^{-1}) is typically dominated by the slow oscillations of modifier cations in their relatively large NBO cages,[62] and indeed the partial VDOS of Y^{3+} only shows a strong broad peak at 140 cm^{-1}. For silicate glasses, the intermediate region (400−800 cm^{-1}) is associated with ring and bending vibrations of T−O−T linkages:[37,63,64]

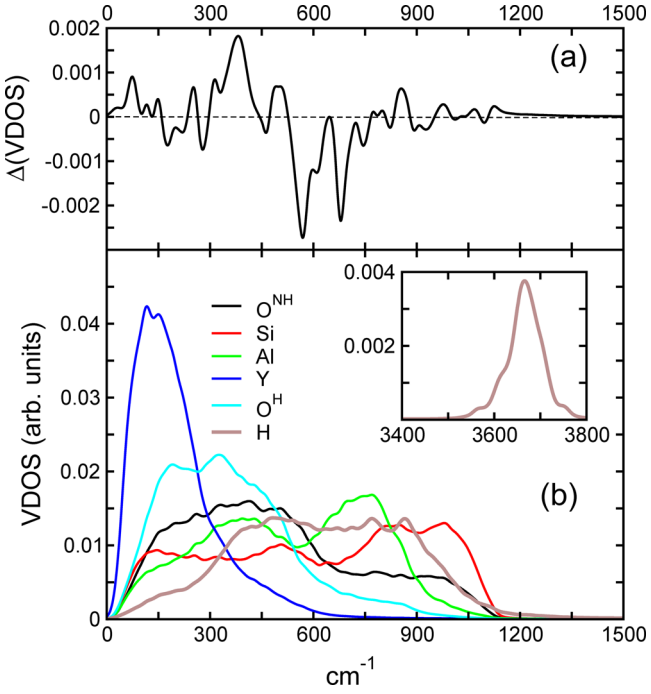

Figure 8. Vibrational density of states for $YAS_{0.3}$ glass: (a) VDOS difference spectrum with respect to the dry glass; (b) partial VDOS for each atomic species.

the partial VDOS functions show that both Si and Al contribute to this region, but the Al vibrations (peaks centered at 400 and 750 cm^{-1}) are red-shifted with respect to Si (500 and 810 cm^{-1}), in agreement with previous vibrational data.[30] The higher-frequency region above 800 cm^{-1} is normally a combination of the stretching modes of various Q_n silicate units:[37,64,65] the figure highlights in fact the dominant contribution of VDOS(Si) in this region. The VDOS of the hydroxyl O^H species denotes coupling with the typical Y and Al vibrations, whereas that with Si is less marked, reflecting the preferential association discussed in the previous sections. The inset in the figure highlights the OH stretching region; in addition to the main peak at 3660 cm^{-1}, there is a lower-frequency shoulder at 3550 cm^{-1} reflecting OH groups hydrogen-bonded to another OH. Both peaks are in good agreement with IR data for aluminosilicate glasses.[28,30] The top panel of Figure 8 reports the difference spectrum ($VDOS_{hydr} - VDOS_{dry}$) of the hydrated glass VDOS, with respect to the total VDOS of the dry glass. Hydration enhances the vibrational intensity in the 300−400 cm^{-1} region, where the main VDOS(O^H) peak is located (Figure 8b). At the same time, the figure shows a significant intensity decrease in the T−O−T vibrational modes between 500 and 750 cm^{-1}: a similar effect of hydration was previously reported for hydrated aluminosilicate glasses and ascribed to structural changes induced by water, with new Al−OH bonds replacing T−O−T linkages.[63] Additional hydration-related characteristic peaks have been reported in the higher frequency region. Peaks at ∼850 and 970 cm^{-1} (also observed in the present difference VDOS) were assigned to Al−OH[31,65] and Si−OH[28] vibrations, respectively, reflecting the formation of these bonds in the hydrated glass. Alternative interpretations linked the increased intensity in this region to changes in the Q_n distributions upon hydration, with a higher density of Al−NBO due to the depolymerization of the Al network.[37] The structural results reported in this work thus

dx.doi.org/10.1021/jp4073203 | J. Phys. Chem. B 2013, 117, 14518−14528

support a combination of both effects as responsible for the hydration-related vibrational changes in this region.

In Figure 9, the VDOS of O^H species is further decomposed into the contributions from free, terminal (Si−OH and Al−OH), and bridging (Si−OH−Al and Al−OH−Al) species. The VDOS of the free OH groups is entirely located below 600 cm^{-1}, reflecting the strong association of these species with Y^{3+} and the corresponding weaker (non-bonded) interaction with Si and Al. OH bonded to Si and Al show in fact significant intensity in the region above 600 cm^{-1}; in particular, the VDOS of (Si−)O^H extends to higher frequencies than that of (Al−)O^H species, a shift in agreement with the experimental results.[30] Bridging OH species present additional features with respect to the terminal OH: in particular, the Al−OH−Al VDOS shows peaks at 580 and 710 cm^{-1} which are not evident in the corresponding Al−OH VDOS, whereas the Si−OH−Al VDOS appears as a combination of the Si−OH and Al−OH vibrations. The top panel of Figure 9 focuses on the O−H stretching region. The main OH peak around 3600 cm^{-1} shows that the O−H stretching of bridging OH species is blue-shifted by up to 50 cm^{-1} compared to that of free and terminal OH. Moreover, each individual band is made of 2−4 sub-bands that reflect hydrogen bonds or other interactions differently affecting the O−H oscillation.[28] Finally, the inset in Figure 9b highlights some residual weak intensity around 2800−3000 cm^{-1}. This appears mainly associated to OH groups bonded to Al. A previous assignment (for an Al-free silicate glass) of a band in this region to silanol groups H-bonded to NBOs[28] suggests that in the present system H-bonded (Al−)OH are responsible for this feature. The latter was also associated to bridging OH groups in hydrogen feldspar $HAlSi_3O_8$,[66] although based on Figure 9a, both bridging and terminal Al-bonded OH groups seem to contribute to it.

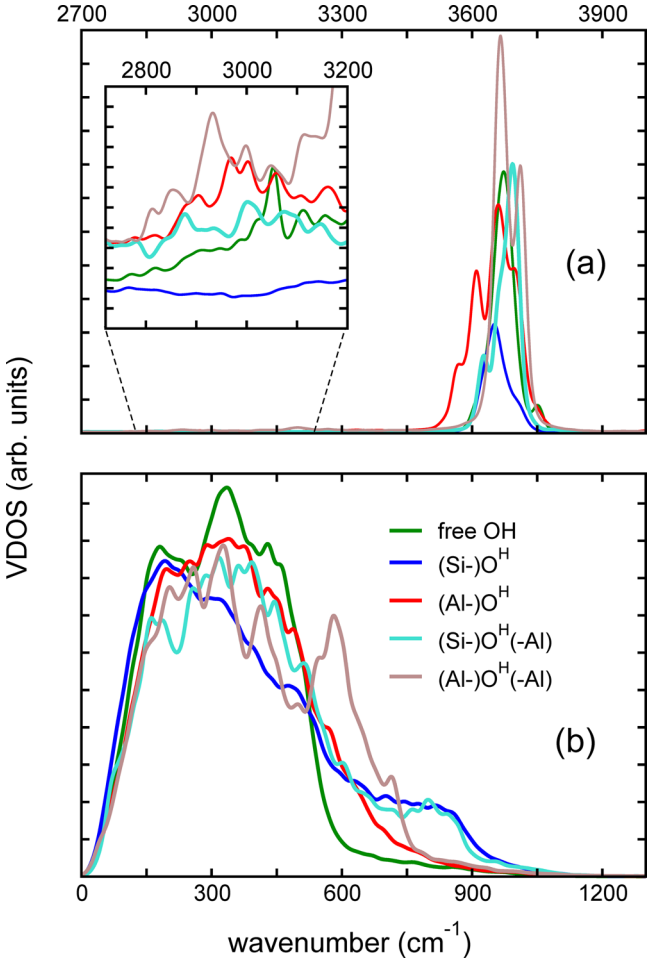

Figure 9. Partial VDOS of the different types of hydroxyl oxygen atoms (O^H) identified in $YAS_{0.3}$.

DISCUSSION AND FINAL REMARKS

The connectivity of the glass network has a central role in determining the glass dissolution rate: a fragmented network with a low connectivity will dissolve faster in an aqueous environment.[9,67] For instance, low-silica bioactive glasses have NC around 2, whereas loss of bioactivity has empirically[68] been associated to NC approaching 3 in higher silica compositions. The central importance of the network connectivity in this context makes it a key structural factor for the possible use of a silica-based glass composition to store radionuclides, either in nuclear waste disposal or for in situ cancer radiotherapy. The incorporation of water in the form of hydroxyl groups in a glass structure is in principle expected to disrupt the glass network: this is based on the assumption that protons act as additional network modifiers[39] and therefore the $O^{2-} \rightarrow 2OH^-$ substitution will break T−O−T bridges either directly (e.g., T−O−T + $OH^- \rightarrow$ T−O^- + T−OH) or indirectly (e.g., T−O···M + $OH^- \rightarrow$ T−OH + M^+, where M^+ is a modifier cation set free in the process and thus able to break another T−O−T bridge). For instance, the depolymerization of the silica network (compared to melt-derived glasses) induced by the wet processing is often reported as one of the possible effects contributing to the extended range of bioactivity of sol−gel glasses.[39] Similarly, a more disrupted YAS network would be less stable in a physiological environment, obviously affecting its performance for radiotherapy. In the short term, a much faster yttrium release in the bloodstream from a rapidly dissolving glass would be a negative factor for the medical applications, which require the highest short-term durability to avoid releasing Y isotopes while they are radioactive. On the other hand, if short-term Y^{3+} release is not significantly affected, the possibility to enhance the long-term (post-radioactive decay of Y) biodegradation of YAS glasses into harmless products represents a very attractive option at present, because the long-term effects of implanted YAS microparticles are unknown. Therefore, it is important to investigate the effects of different hydration levels on the glass structure. The present simulations show that the disruptive effect of OH^- on the glass network acts differently on the silicate and aluminate connectivity. Overall, the silicate NC is unaffected by hydration, while the Al NC decreases as expected. This occurs because OH^- mainly happens to break Si−Al cross-links (possibly weaker than Si−Si and Al−Al), which dominate the Al connectivity, but not the Si connectivity (Figure 5). Another reason why the network depolymerization is less than expected has to do with the presence of "free" OH groups highlighted by the simulations: as these are not directly bonded to either Si or Al, free OH's do not affect the Si/Al ability to form T−O−T bridges. The driving force leading to the presence of free OH groups is the strong Y−OH interaction, which leads to the formation of stable aggregates of Y^{3+} and OH^- ions, separated from the aluminosilicate network. An example of one of these aggregates is visualized in Figure 10. The marked Y−OH association with formation of nanosegregated Y−OH regions could in principle accelerate the dissolution process of "solvated" yttrium ions and

dx.doi.org/10.1021/jp4073203 | J. Phys. Chem. B 2013, 117, 14518−14528

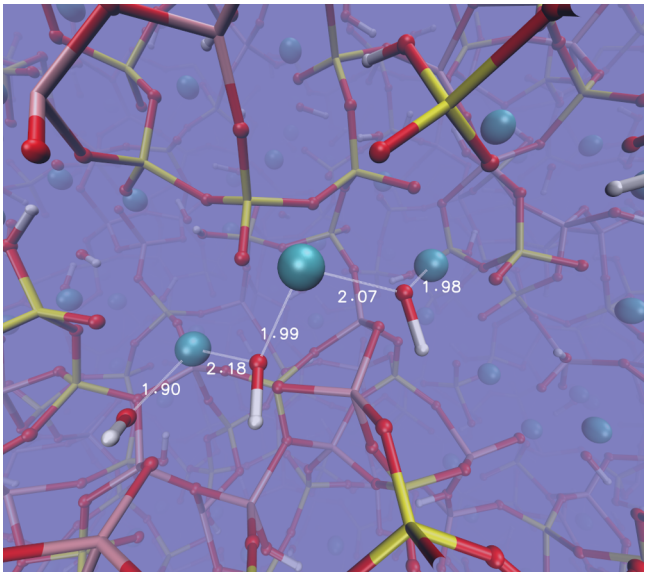

Figure 10. A snapshot extracted from the MD trajectory of $YAS_{0.3}$, highlighting an aggregate of three "free" OH (i.e., not bonded to Si or Al) in close association with three yttrium ions (spheres). Si, Al, O, Y, and H are colored yellow, orange, red, cyan, and white, respectively.

their release from the glass matrix into the surrounding environment. The potential effect of OH solvation on directly enhancing the Y solubility may balance the reduced impact of OH^- on the connectivity of the glass matrix itself, discussed before. At the same time, the negative correlation between Y−Y clustering and the YAS glass solubility, recently highlighted for the dry glass, should also be taken into account for predicting the dissolution properties of the hydrated glasses.[12]

The present results can be linked to the previous experimental findings for hydrated aluminosilicate glasses discussed in the Introduction. The behavior of OH groups found here for the YAS17 glass recalls that previously reported for Na−, Ca−, and Mg−aluminosilicate glasses,[33−35] which showed the concomitant formation of Si−OH, Al−OH, and free OH species, at variance with other studies reporting that no bonds with either Si or Al are formed.[32] The relatively high abundance of free OH species that we detect in YAS17 also agrees with the experimental suggestion that their weight increases when the glass contains modifier cations of higher field strength, such as Y^{3+}.[33,36] The models show that hydroxyl association to the network formers Si and Al has different effects: in the first case, the coordination shell and the average Si connectivity are not modified, whereas in the case of Al there is a slight increase in both, which reflects the higher tendency of Al to be found in non-tetrahedral environments in these glasses,[57] and also agrees with the slight increase in Al coordination with water amount, previously reported.[33,69] The fraction of OH bonded to Al in hydrous aluminosilicate glasses containing low water amounts was previously shown to increase with the Al/(Al + Si) fraction of the glass.[70] An Al-bonded fraction of OH between 0.3 and 0.4 was found for an Al/(Al + Si) ratio similar to that of the YAS17 glass, which is in good agreement with the corresponding Al−OH fractions reported in Table 4, also considered that the present composition contains Y_2O_3 instead of Na_2O as in the experiments. The simulations also highlighted significant clustering of the free OH species, as suggested by diffraction data,[37] but not detected in other experimental studies.[19] The high Y^{3+}−OH affinity appears to be the driving force for the separation of OH clusters in the YAS case: the nature of the modifier cation may be the key factor in determining the tendency to form free-OH domains in the glass.

Thermodynamical calculations[63] and NMR chemical shift values[33] highlighted stronger Si−OH than Al−OH interactions, which would also reflect the higher acidity of Si^{4+}. On the other hand, fluoride (whose structural role in the glass is considered similar to that of OH^-[30]) shows a preference for Al in silicate glasses, over Si and Na.[71] The balance between Si−OH and Al−OH interactions thus appears rather delicate, and affected by factors such as the glass composition, the chemical species present, and then also the water concentration. For low water amounts, the thermodynamical/acidity considerations seem to prevail, leading to the initial preferential Si:OH association that we observe. For higher water amounts, there seemingly are other factors that come into play besides those above, which cause the OH distribution to shift over to Al. Further work would be needed to identify these factors.

In conclusion, the present simulations have highlighted that the incorporation of OH groups in a yttrium-doped aluminosilicate glass matrix introduces structural effects which may influence the dissolution behavior of the glass in nonobvious ways. On one hand, the uneven distribution of OH groups between Si and Al and their different effect on cross- and self- T−O−T bridges only disrupts the Al connectivity but not the Si one. At the same time, the formation of YOH-rich regions separated from the Si−Al matrix results in a significant fraction of "free" OH groups which do not directly alter the strength of the glass network and the corresponding biodegradability but could affect the yttrium release rate. The identification of these fundamental effects is the first step toward a rationalization of the properties of hydrated YAS glasses for biomedical applications. Next steps will involve looking into how their balance ultimately determines the biodegradation mechanism, and how it could be altered to control the material performances in practical applications.

AUTHOR INFORMATION

Corresponding Author

*E-mail: a.tilocca@ucl.ac.uk.

Notes

The authors declare no competing financial interest.

ACKNOWLEDGMENTS

The UK's Royal Society is gratefully acknowledged for financial support (University Research Fellowship).

REFERENCES

(1) Hench, L. L.; Polak, J. M. Third-Generation Biomedical Materials. *Science* **2002**, *295* (5557), 1014−1017.

(2) Jones, J. R. Review of bioactive glass: From Hench to hybrids. *Acta Biomater.* **2013**, *9* (1), 4457−4486.

(3) Michalske, T. A.; Bunker, B. C. Slow fracture model based on strained silicate structures. *J. Appl. Phys.* **1984**, *56* (10), 2686−2693.

(4) Cailleteau, C.; Angeli, F.; Devreux, F.; Gin, S.; Jestin, J.; Jollivet, P.; Spalla, O. Insight into silicate-glass corrosion mechanisms. *Nat. Mater.* **2008**, *7* (12), 978−983.

(5) Erbe, E. M.; Day, D. E. Chemical durability of Y2O3−Al2O3-SiO2 glasses for the in vivo delivery of beta radiation. *J. Biomed. Mater. Res.* **1993**, *27* (10), 1301−1308.

(6) Ho, S.; Lau, W. Y.; Leung, T. W. T.; Johnson, P. J. Internal radiation therapy for patients with primary or metastatic hepatic cancer. *Cancer* **1998**, *83* (9), 1894−1907.
(7) Kawashita, M. Ceramic microspheres for in situ radiotherapy of cancer. *Mater. Sci. Eng., C* **2002**, *22* (1), 3−8.
(8) Gaba, R.; Lewandowski, R.; Kulik, L.; Riaz, A.; Ibrahim, S.; Mulcahy, M.; Ryu, R.; Sato, K.; Gates, V.; Abecassis, M.; Omary, R.; Baker, T.; Salem, R. Radiation Lobectomy: Preliminary Findings of Hepatic Volumetric Response to Lobar Yttrium-90 Radioembolization. *Ann. Surg. Oncol.* **2009**, *16* (6), 1587−1596.
(9) Tilocca, A. Models of structure, dynamics and reactivity of bioglasses: a review. *J. Mater. Chem.* **2010**, *20* (33), 6848−6858.
(10) Christie, J. K.; Tilocca, A. Aluminosilicate Glasses As Yttrium Vectors for in situ Radiotherapy: Understanding Composition-Durability Effects through Molecular Dynamics Simulations. *Chem. Mater.* **2010**, *22* (12), 3725−3734.
(11) Christie, J. K.; Tilocca, A. Short-Range Structure of Yttrium Alumino-Silicate Glass for Cancer Radiotherapy: Car−Parrinello Molecular Dynamics Simulations. *Adv. Eng. Mater.* **2010**, *12* (7), B326−B330.
(12) Christie, J. K.; Tilocca, A. Molecular Dynamics Simulations and Structural Descriptors of Radioisotope Glass Vectors for In Situ Radiotherapy. *J. Phys. Chem. B* **2012**, *116* (41), 12614−12620.
(13) Christie, J. K.; Malik, J.; Tilocca, A. Bioactive glasses as potential radioisotope vectors for in situ cancer therapy: investigating the structural effects of yttrium. *Phys. Chem. Chem. Phys.* **2011**, *13* (39), 17749−17755.
(14) Tilocca, A.; Cormack, A. N.; de Leeuw, N. H. The structure of bioactive silicate glasses: New insight from molecular dynamics simulations. *Chem. Mater.* **2007**, *19* (1), 95−103.
(15) Jund, P.; Kob, W.; Jullien, R. Channel diffusion of sodium in a silicate glass. *Phys. Rev. B* **2001**, *64* (13), 134303.
(16) Tilocca, A. Sodium migration pathways in multicomponent silicate glasses: Car–Parrinello molecular dynamics simulations. *J. Chem. Phys.* **2010**, *133* (1), 014701−10.
(17) Christie, J. K.; Tilocca, A. *J. Mater. Chem.* **2012**, *22*, 12023−12031.
(18) Dingwell, D. B.; Mysen, B. O. Effects of water and fluorine on the viscosity of albite melt at high pressure: a preliminary investigation. *Earth Planet. Sci. Lett.* **1985**, *74* (2−3), 266−274.
(19) Eckert, H.; Yesinowski, J. P.; Silver, L. A.; Stolper, E. M. Water in silicate glasses: quantitation and structural studies by proton solid echo and magic angle spinning NMR methods. *J. Phys. Chem.* **1988**, *92* (7), 2055−2064.
(20) Batyrev, I. G.; Tuttle, B.; Fleetwood, D. M.; Schrimpf, R. D.; Tsetseris, L.; Pantelides, S. T. Reactions of Water Molecules in Silica-Based Network Glasses. *Phys. Rev. Lett.* **2008**, *100* (10), 105503.
(21) Berger, S.; Tomozawa, M. Water diffusion into a silica glass optical fiber. *J. Non-Cryst. Solids* **2003**, *324* (3), 256−263.
(22) Shin, D. W.; Tomozawa, M. Effects of fictive temperature and water content on electrical conductivity of silica glasses. *J. Non-Cryst. Solids* **1996**, *203* (0), 262−267.
(23) García, N. J.; Ingram, M. D.; Bazán, J. C. Ion transport in hydrated sodium silicates (water glasses) of varying water content. *Solid State Ionics* **2002**, *146* (1−2), 113−122.
(24) Davis, K. M.; Tomozawa, M. Water diffusion into silica glass: Structural changes in silica glass and their effect on water solubility and diffusivity. *J. Non-Cryst. Solids* **1995**, *185* (3), 203−220.
(25) Riemer, T.; Schmidt, B.; Behrens, H.; Dupree, R. H2O/OH ratio determination in hydrous aluminosilicate glasses by static proton NMR and the effect of chemical shift anisotropy. *Solid State Nucl. Magn. Reson.* **2000**, *15* (4), 201−207.
(26) Zotov, N.; Keppler, H.; Hannon, A. C.; Soper, A. K. The effect of water on the structure of silicate glasses — A neutron diffraction study. *J. Non-Cryst. Solids* **1996**, *202* (1−2), 153−163.
(27) Zhang, Y.; Stolper, E. M.; Wasserburg, G. J. Diffusion of water in rhyolitic glasses. *Geochim. Cosmochim. Acta* **1991**, *55* (2), 441−456.
(28) Davis, K. M.; Tomozawa, M. An infrared spectroscopic study of water-related species in silica glasses. *J. Non-Cryst. Solids* **1996**, *201* (3), 177−198.
(29) Freund, F. Solubility Mechanisms of H2o in Silicate Melts at High-Pressures and Temperatures - a Raman-Spectroscopic Study - Discussion. *Am. Mineral.* **1982**, *67* (1−2), 153−154.
(30) Mysen, B. O.; Virgo, D. Volatiles in silicate melts at high pressure and temperature: 2. Water in melts along the join NaAlO2−SiO2 and a comparison of solubility mechanisms of water and fluorine. *Chem. Geol.* **1986**, *57* (3−4), 333−358.
(31) Sykes, D.; Kubicki, J. D. A model for H2O solubility mechanisms in albite melts from infrared spectroscopy and molecular orbital calculations. *Geochim. Cosmochim. Acta* **1993**, *57* (5), 1039−1052.
(32) Kohn, S. C.; Dupree, R.; Smith, M. E. A multinuclear magnetic resonance study of the structure of hydrous albite glasses. *Geochim. Cosmochim. Acta* **1989**, *53* (11), 2925−2935.
(33) Xue, X.; Kanzaki, M. Al coordination and water speciation in hydrous aluminosilicate glasses: Direct evidence from high-resolution heteronuclear 1H−27Al correlation NMR. *Solid State Nucl. Magn. Reson.* **2007**, *31* (1), 10−27.
(34) Xue, X. Y. Water speciation in hydrous silicate and aluminosilicate glasses: Direct evidence from Si-29-H-1 and Al-27-H-1 double-resonance NMR. *Am. Mineral.* **2009**, *94* (2−3), 395−398.
(35) Zeng, Q.; Nekvasil, H.; Grey, C. P. Proton Environments in Hydrous Aluminosilicate Glasses: A 1H MAS, 1H/27Al, and 1H/23Na TRAPDOR NMR Study. *J. Phys. Chem. B* **1999**, *103* (35), 7406−7415.
(36) Xue, X.; Kanzaki, M. Dissolution mechanisms of water in depolymerized silicate melts: Constraints from 1H and 29Si NMR spectroscopy and ab initio calculations. *Geochim. Cosmochim. Acta* **2004**, *68* (24), 5027−5057.
(37) Zotov, N.; Yanev, Y.; Epelbaum, M.; Konstantinov, L. Effect of water on the structure of rhyolite glasses - X-ray diffraction and Raman spectroscopy studies. *J. Non-Cryst. Solids* **1992**, *142* (0), 234−246.
(38) Mead, R. N.; Mountjoy, G. Modeling the Local Atomic Structure of Bioactive Sol−Gel-Derived Calcium Silicates. *Chem. Mater.* **2006**, *18* (17), 3956−3964.
(39) Jones, J. R. Sol-Gel Derived Glasses for Medicine. In *Bio-Glasses*; John Wiley & Sons, Ltd: Chichester, 2012; pp 29−44.
(40) Rao, N. Z.; Gelb, L. D. Molecular Dynamics Simulations of the Polymerization of Aqueous Silicic Acid and Analysis of the Effects of Concentration on Silica Polymorph Distributions, Growth Mechanisms, and Reaction Kinetics. *J. Phys. Chem. B* **2004**, *108* (33), 12418−12428.
(41) Bhattacharya, S.; Kieffer, J. Molecular Dynamics Simulation Study of Growth Regimes during Polycondensation of Silicic Acid: from Silica Nanoparticles to Porous Gels. *J. Phys. Chem. C* **2008**, *112* (6), 1764−1771.
(42) Smith, W.; Forester, T. R. DL_POLY_2.0: A general-purpose parallel molecular dynamics simulation package. *J. Mol. Graphics* **1996**, *14* (3), 136−141.
(43) Tilocca, A.; de Leeuw, N. H.; Cormack, A. N. Shell-model molecular dynamics calculations of modified silicate glasses. *Phys. Rev. B* **2006**, *73* (10), 104209.
(44) Tilocca, A.; Cormack, A. N.; de Leeuw, N. H. The formation of nanoscale structures in soluble phosphosilicate glasses for biomedical applications: MD simulations. *Faraday Discuss.* **2007**, *136* (0), 45−55.
(45) Baram, P. S.; Parker, S. C. Atomistic simulation of hydroxide ions in inorganic solids. *Philos. Mag. B* **1996**, *73* (1), 49−58.
(46) Schroder, K. P.; Sauer, J.; Leslie, M.; Catlow, C. R. A.; Thomas, J. M. *Chem. Phys. Lett.* **1992**, *188* (3−4), 320−325.
(47) Gale, J. D.; Rohl, A. L. The General Utility Lattice Program (GULP). *Mol. Simul.* **2003**, *29* (5), 291−341.
(48) Zokaie, M.; Olsbye, U.; Lillerud, K. P.; Swang, O. Stabilization of Silicon Islands in Silicoaluminophosphates by Proton Redistribution. *J. Phys. Chem. C* **2012**, *116* (13), 7255−7259.
(49) Verheyen, E.; Joos, L.; Van Havenbergh, K.; Breynaert, E.; Kasian, N.; Gobechiya, E.; Houthoofd, K.; Martineau, C.; Hinterstein,

M.; Taulelle, F.; Van Speybroeck, V.; Waroquier, M.; Bals, S.; Van Tendeloo, G.; Kirschhock, C. E. A.; Martens, J. A. Design of zeolite by inverse sigma transformation. *Nat. Mater.* **2012**, *11* (12), 1059−1064.
(50) Chizallet, C.; Raybaud, P. Pseudo-Bridging Silanols as Versatile Brønsted Acid Sites of Amorphous Aluminosilicate Surfaces. *Angew. Chem., Int. Ed.* **2009**, *48* (16), 2891−2893.
(51) Mitchell, P. J.; Fincham, D. Shell-Model Simulations by Adiabatic Dynamics. *J. Phys.: Condens. Matter* **1993**, *5* (8), 1031−1038.
(52) Mahadevan, T. S.; Garofalini, S. H. Dissociative Chemisorption of Water onto Silica Surfaces and Formation of Hydronium Ions. *J. Phys. Chem. C* **2008**, *112* (5), 1507−1515.
(53) Due to the higher weight of the more abundant non-hydroxyl (Onh) species, the peak in the bottom panel of Figure 2 always remains centered at the shorter (Si,Al)−Onh distance. Because the bottom-panel rdf is averaged over both Onh and Oh, the increasing contribution from (Si, Al)−Oh (middle panel) is subtracted from the main shorter-distance peak, resulting in the peak decrease with OH amount, at variance with the top panel where the (Si, Al)−Oh distances do not contribute and do not remove intensity from the (Si, Al)−Onh peak.
(54) Martin, R. A.; Salmon, P. S.; Carroll, D. L.; Smith, M. E.; Hannon, A. C. Structure and thermal properties of yttrium aluminophosphate glasses. *J. Phys.: Condens. Matter* **2008**, *20* (11), 115204.
(55) Du, J.; Benmore, C., J.; Corrales, R.; Hart, R., T.; Weber, J. K. R. A molecular dynamics simulation interpretation of neutron and x-ray diffraction measurements on single phase Y 2 O 3 −Al 2 O 3 glasses. *J. Phys.: Condens. Matter* **2009**, *21* (20), 205102.
(56) Florian, P.; Sadiki, N.; Massiot, D.; Coutures, J. P. 27Al NMR Study of the Structure of Lanthanum- and Yttrium-Based Aluminosilicate Glasses and Melts. *J. Phys. Chem. B* **2007**, *111* (33), 9747−9757.
(57) Iftekhar, S.; Pahari, B.; Okhotnikov, K.; Jaworski, A.; Stevensson, B.; Grins, J.; Edén, M. Properties and Structures of RE2O3−Al2O3−SiO2 (RE = Y, Lu) Glasses Probed by Molecular Dynamics Simulations and Solid-State NMR: The Roles of Aluminum and Rare-Earth Ions for Dictating the Microhardness. *J. Phys. Chem. C* **2012**, *116* (34), 18394−18406.
(58) Strnad, Z. Role of the glass phase in bioactive glass-ceramics. *Biomaterials* **1992**, *13* (5), 317−321.
(59) Tilocca, A.; Cormack, A. N. Structural Effects of Phosphorus Inclusion in Bioactive Silicate Glasses. *J. Phys. Chem. B* **2007**, *111* (51), 14256−14264.
(60) The corresponding uniform distribution number decreases by 1 when $A = B$.
(61) Fois, E.; Gamba, A.; Tilocca, A. Structure and Dynamics of the Flexible Triple Helix of Water inside VPI-5 Molecular Sieves. *J. Phys. Chem. B* **2002**, *106* (18), 4806−4812.
(62) Merzbacher, C. I.; White, W. B. The Structure of Alkaline-Earth Aluminosilicate Glasses as Determined by Vibrational Spectroscopy. *J. Non-Cryst. Solids* **1991**, *130* (1), 18−34.
(63) Mysen, B. O.; Virgo, D. Volatiles in silicate melts at high pressure and temperature: 1. Interaction between OH groups and Si4+, Al3+, Ca2+, Na+ and H+. *Chem. Geol.* **1986**, *57* (3−4), 303−331.
(64) Arcos, D.; Greenspan, D. C.; Vallet-Regí, M. Influence of the Stabilization Temperature on Textural and Structural Features and Ion Release in SiO2−CaO−P2O5 Sol−Gel Glasses. *Chem. Mater.* **2002**, *14* (4), 1515−1522.
(65) McMillan, P. Structural Studies of Silicate-Glasses and Melts - Applications and Limitations of Raman-Spectroscopy. *Am. Mineral.* **1984**, *69* (7−8), 622−644.
(66) Behrens, H.; Muller, G. An Infrared Spectroscopic Study of Hydrogen Feldspar ($HAlSi_3O_8$). *Mineral. Mag.* **1995**, *59* (394), 15−24.
(67) Tilocca, A. Structural models of bioactive glasses from molecular dynamics simulations. *Proc. R. Soc. London, Ser. A* **2009**, *465* (2104), 1003−1027.
(68) Hill, R. An alternative view of the degradation of bioglass. *J. Mater. Sci. Lett.* **1996**, *15* (13), 1122−1125.
(69) Manning, D. A. C.; Hamilton, D. L.; Henderson, C. M. B.; Dempsey, M. J. The Probable Occurrence of Interstitial Al in Hydrous, F-Bearing and F-Free Aluminosilicate Melts. *Contrib. Mineral. Petrol.* **1980**, *75* (3), 257−262.
(70) Malfait, W. J.; Xue, X. Y. The nature of hydroxyl groups in aluminosilicate glasses: Quantifying Si-OH and Al-OH abundances along the SiO2-NaAlSiO4 join by H-1, Al-27-H-1 and Si-29-H-1 NMR spectroscopy. *Geochim. Cosmochim. Acta* **2010**, *74* (2), 719−737.
(71) Schaller, T.; Dingwell, D. B.; Keppler, H.; Knöller, W.; Merwin, L.; Sebald, A. Fluorine in silicate glasses: A multinuclear nuclear magnetic resonance study. *Geochim. Cosmochim. Acta* **1992**, *56* (2), 701−707.